Shear-Induced Network-to-Network Transition in a Block Copolymer Melt

Eric W. Cochran and Frank S. Bates*

Department of Chemical Engineering and Materials Science, University of Minnesota, Minneapolis, Minnesota 55455, USA

(Received 19 March 2004; published 20 August 2004)

A tricontinuous $(10, 3)c$ network phase is documented in a poly(cyclohexylethylene-*b*-ethylethylene-*b*-ethylene) triblock copolymer melt based on small-angle x-ray scattering. Application of shear transforms the self-assembled soft material into a single crystal $(10, 3)d$ network while preserving the short-range threefold connector geometry. Long-range topological restructuring reduces the space group symmetry, from *Fddd* to *Pnna*, maintaining orthorhombic lattice symmetry. Both phases are stable to long time annealing, indicative of nearly degenerate free energies and prohibitive kinetic barriers.

DOI: 10.1103/PhysRevLett.93.087802 PACS numbers: 61.41.+e, 61.10.Eq, 61.12.Ex, 61.46.+w

Flow and deformation, important in the processing of many materials, are particularly influential in defining the structure of soft condensed matter. For example, the morphology of surfactant mixtures [1,2], liquid crystals [3], colloids [4], polymeric bicontinuous microemulsions [5], polymer solutions and blends [6], and block copolymers [7] is coupled inextricably to the symmetry and intensity of applied flow fields. Steady-state structure reflects a compromise between the preferred phase in static equilibrium and the ability to dissipate stress, produced by deformation within a characteristic time scale.

One- and two-dimensional structures (e.g., layers and cylinders) readily accommodate large shear strains, through domain alignment over macroscopic dimensions [1–3,7,8]. However, this pathway is not available to three-dimensional structures, and particularly triply periodic soft materials, which behave as elastic solids in the limit of small strains. The effects of disruptive flows are complicated [5,9–13]. For instance, Krishnan *et al.* discovered a progression of structural adaptations with increasing shear rate in a polymeric bicontinuous microemulsion, culminating in macroscopic phase separation [5]. In ternary oil-water-surfactant mixtures, shear can convert the cubic gyroid phase to the lamellar L_3 phase [2]. Both examples illustrate how three-dimensional structures minimize stored energy by forming continuous channels, or slip planes, when deformed.

Triply periodic diblock copolymer melts are known to convert to lower symmetry states under the influence of strong flow fields. The Q^{230} (gyroid) phase transforms to a metastable hexagonally perforated layer morphology [14,15], while spheres packed on a bcc lattice undergo a reversible transition to hexagonally packed cylinders [9], under the influence of large amplitude reciprocating shear. In both cases flow transforms the soft solid into a lower dimensional crystal with macroscopic alignment.

Until recently, all network structures encountered in soft materials have been cubic, a phenomenon attributable to the isotropic nature of the forces that drive self-assembly. The first exception to this observation was published by Bailey *et al.* with the identification of a noncubic network morphology, tentatively assigned to the *Fddd* space group (No. 70), in a number of poly(isoprene-*b*-styrene-*b*-ethyleneoxide) (ISO) triblock copolymers [16]. Epps *et al.* recently confirmed this model using additional ISO compositions, establishing O^{70}, an orthorhombic $(10, 3)c$ network morphology, as an equilibrium phase in *ABC* block copolymers [17]. [A (10, 3) network contains a regular array of 10-node loops of threefold connectors. Wells [18] has identified seven different uniform (10, 3) networks.] Phase formation in linear *ABC* triblock copolymer melts is particularly delicate; the balance between minimization of interfacial contact between dissimilar blocks (enthalpy) and the optimization of chain packing (entropy) gives rise to numerous candidate structures that differ only slightly in free energy. The present study was motivated by the supposition that the processing behavior of orthorhombic O^{70} should be markedly different from that of the familiar cubic solids. To test this hypothesis, we examined sample CE_EE-3 from Ref. [19], a poly(cyclohexylethylene-*b*-ethylethylene-*b*-ethylene) triblock copolymer with mass fractions $C/E_E/E = 0.29/0.49/0.22$, $M_n = 30\,500$ Da, and $M_w/M_n = 1.08$.

Figure 1 shows synchrotron small-angle x-ray scattering (SAXS) from CE_EE-3. These experiments were conducted on the DND-CAT at the Advanced Photon Source at Argonne National Laboratory, with wavelength $\lambda = 0.827$ Å and a sample-to-detector distance SDD = 501 cm. Two-dimensional data were accumulated on a Mar CCD area detector. Scattering angle θ was converted to wave vector modulus $q = 4\pi/\lambda \sin(\theta/2)$. Temperature was controlled with a Linkham DSC under helium purge. CE_EE-3 was heated to 10 °C above the order-to-disorder transition temperature ($T_{ODT} = 180$ °C), and then cooled to 178 °C. Annealing at this temperature limits nucleation and encourages the growth of a discrete number of large, well-defined grains. This treatment enabled the collection

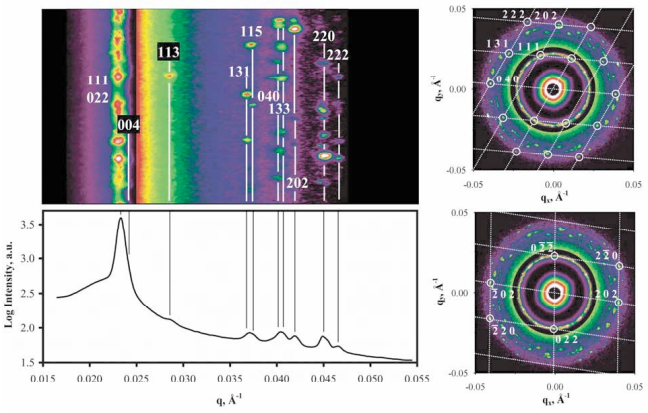

FIG. 1 (color). SAXS patterns from CE_EE-3, ordered by cooling a disordered melt to 178 °C, slightly below T_{ODT}, and extended annealing. Lower left: Azimuthally integrated 2D data. Upper left: Polar representation (azimuthal angle vs q) of the 2D data. Upper and lower right: The 2D data with indexing for single grains according to the *Fddd* assignment. Dashed grids identify the associated reciprocal lattices. All contour plots use a different intensity scale for $q < 0.26$ Å^{-1} so that both principle and high-order reflections are visible.

of a multigrain spot diffraction pattern with multiple orders of Bragg reflections; several representations of these data appear in Fig. 1. The upper-left panel displays the 2D data in polar coordinates (azimuthal angle vs q), while the azimuthally integrated intensity appears directly below. The peak locations conform to an *Fddd* space group assignment, with lattice constants $a = 0.30c$, $b = 0.60c$, and $c = 100$ nm. The right panels exhibit the 2D data with two sets of indexed *Fddd* reflections, shown with the appropriate reciprocal lattices, which originate from single grains.

Predictably, the ISO and CE_EE systems share a common set of equilibrium phases. Both have symmetrically balanced interfacial tensions, i.e., $\chi_{AB} \approx \chi_{BC} \ll \chi_{AC}$, where χ_{ij} is a binary segment-segment interaction parameter. At comparable compositions, and near the order-disorder transition temperature, each forms the O^{70} phase. Because of a larger molar mass, and higher entanglement density, CE_EE-3 is a superior candidate for studying the susceptibility of O^{70} to shear.

CE_EE-3 was compression molded at 170 °C at 500 psi for 10 min to a 0.5 mm thickness and cut to fit a 25 mm × 25 mm × 0.5 mm aluminum shear cell. The polymer was heated to 200 °C under dynamic vacuum and annealed at 160 °C for 24 h, and then placed in a helium purged reciprocating steady-shear apparatus, located on the NG7 30m beam line at the NIST Center for Neutron Research [20]. The sample was heated to 190 °C, above T_{ODT}, and cooled to 160 °C prior to activating the shear apparatus; this thermal treatment yields an isotropic distribution of *Fddd* grains with 1D SAXS data equivalent to those in Fig. 1. During the shear experiment, we collected *in situ* small-angle neutron scattering (SANS) data at 2 min intervals using neutrons with $\lambda = 6$ Å, $\Delta\lambda/\lambda = 0.15$, and SDD = 7.5 m. The neutron beam was parallel to the shear gradient direction (b axis in Fig. 2), and a shear rate of $\dot{\gamma} = 5$ s^{-1} (sawtooth displacement profile) with strain amplitude $|\gamma| = 600\%$ was employed. Application of shear rapidly produced individual reflections, and after 6 min the peak locations and intensities achieved a steady state. The SANS pattern shown in Fig. 2 was collected after 10 min and represents the steady-state structure.

The SANS result contains a number of Bragg peaks, situated on a single reciprocal space lattice, that satisfy the extinction rules for several space groups, including *Fddd*. To unambiguously determine the space group symmetry, the specimen was cooled to room temperature and then sectioned so that an x-ray beam could be directed coincident with the orthogonal axes defined by the deformation geometry: the shear (a), shear gradient (b), and vorticity (c) directions (Fig. 2). Each section was heated under dynamic vacuum to 160 °C, annealed for 12 h, and then cooled to 115 °C to maximize the scattering contrast. These experiments were conducted at the University of Minnesota Institute of Technology Characterization Facility using an instrument described in Ref. [16]; Cu $K\alpha$ radiation with $\lambda = 1.54$ Å was used and SDD = 230 cm. The resultant SAXS patterns (Fig. 3), with multiple orders of reflections and systematic extinctions, con-

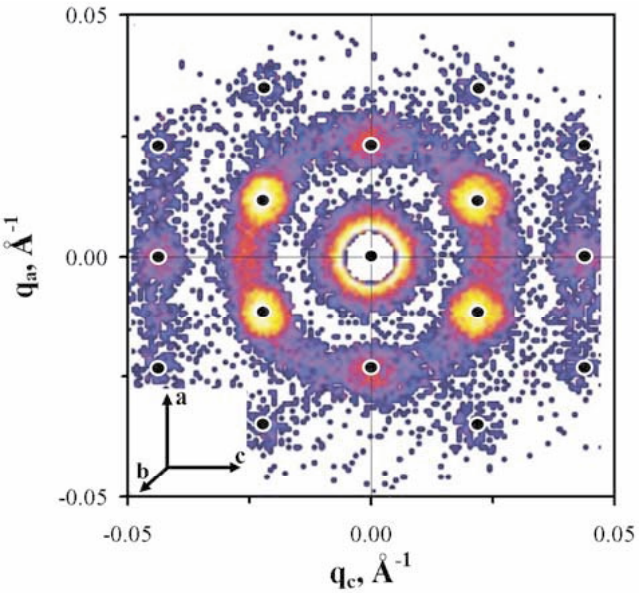

FIG. 2 (color). Steady-state *in situ* SANS from CE_EE-3 at 160 °C, after 10 min of reciprocating shear. The neutron beam was directed along the shear gradient b direction as depicted by the coordinate system diagram. The shear direction corresponds to the a axis, and the vorticity direction the c axis. The symbols correspond to reflections allowed by *Pnna* symmetry according to the indexing scheme of Fig. 3(b).

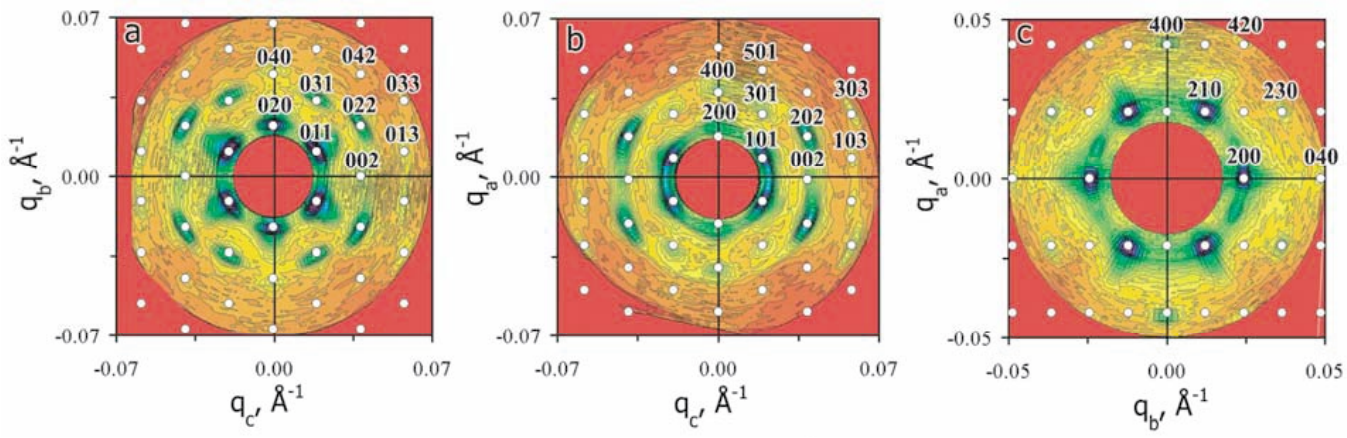

FIG. 3 (color). The 2D SAXS patterns from annealed, macroscopically shear-aligned CE_EE-3. The symbols indicate where *Pnna* reflections are allowed. The beam is parallel to (a) the *a* direction (shear), (b) the *b* direction (shear gradient), and (c) the *c* direction (vorticity).

form uniquely to another orthorhombic space group, *Pnna* (No. 52), with lattice constants $a = 2.00c$, $b = 1.73c$, $c = 30.7$ nm.

Clearly, shear has induced a phase transition from a polycrystalline orthorhombic phase (O^{70}) to a new, nearly single crystalline, orthorhombic structure that we denote O^{52}. To model this altered structure, we constructed a density field with *Pnna* symmetry using the Fourier synthesis technique previously applied to the *Fddd* state [17] and described in the literature [21]. Block domain interfaces (C/E_E and E_E/E) were modeled as constant density level sets, with the isovalue of each surface chosen to duplicate the correct volume fractions according to CE_EE-3. Figure 4 (lower panels) shows unit cells of the composite *Fddd* and *Pnna* structures according to the level set constructions. The structure of the triply periodic O^{52} surfaces is topologically equivalent to the $(10, 3)d$ network class, which is known to belong to the *Pnna* space group [18]. Figure 4 (upper panels) shows the domain connectivity of the initial *Fddd* structure and the transformed *Pnna* network, represented as ball-and-stick models. The nodes of each model correspond to Wyckoff position 16*g* and 8*e*, of the *Fddd* and *Pnna* space groups, respectively. There are various connector geometries that satisfy the symmetry conditions of each site. In general, the $(10, 3)c$ connector must be planar and contain mirror planes orthogonal to the [110] and $[1\bar{1}0]$ directions; threefold connector symmetry is not possible with the O^{70} lattice dimensions. The $(10, 3)d$ junction has lower symmetry than that of the $(10, 3)c$ net, with a range of possible bond lengths and angles. The network lattice representations in the upper panels of Fig. 4 show just a single example, where the O^{52} and O^{70} share the same connector geometry.

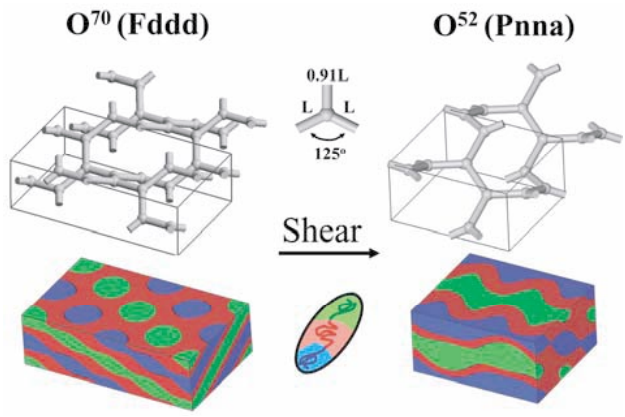

FIG. 4 (color). Upper panel: Ball-and-stick representations of the $(10, 3)c$ and $(10, 3)d$ network topologies (2 unit cells, the wire-frame box demarks the unit cell boundary). Here, both structures are built from geometrically equivalent planar trivalent connectors, with the longest strut length $L = 18.5$ nm for both (note that this geometry is not unique, and that symmetry does allow the O^{52} and O^{70} connectors to differ). Lower panel: Simulated space filling morphologies for a unit cell of the O^{70} and O^{52} phases in CE_EE-3. The shaded oval illustrates the orientation of a polymer chain with respect to the surfaces.

Here we note the congruence in wave vector, but not relative intensity, between the SANS collected along the *b* axis *in situ* during shear processing, and the SAXS taken from the same direction after extended annealing (locations of symbols on Fig. 2 correspond precisely to those in Fig. 3(b)]. This is an indication that while the steady-state sheared structure shares a subset of the symmetries of O^{52}, the transient morphology does not represent the final annealed state. Rather, the SANS data represent the *average* symmetries of the system, a shear-stable configuration that provides for microphase separation while simultaneously dissipating stress.

Shear destabilizes the O^{70} phase (presumably lacking a slip plane that relaxes stress) leading to an intermediate

state of order. Cessation of flow returns the system to a solid state. However, rather than readopting the O^{70} morphology, a kinetically facile transition converts the intermediate sheared state to the O^{52} network (Fig. 3). We believe O^{52} to be metastable, since O^{70} always forms upon cooling below T_{ODT} under quiescent conditions. A combination of nearly degenerate free energies and a prohibitive kinetic barrier inhibits reversal of the O^{70} to O^{52} transition even after annealing at elevated temperature for several days. These data suggest that on a local level the O^{52} and O^{70} states should be nearly indistinguishable; this may be reflected through a common trivalent connector geometry from which each net is assembled (as is illustrated in Fig. 4). Accordingly, the local chain packing and interfacial contributions to the O^{52} and O^{70} free energy would be quite similar. However, at longer length scales these connectors tile space in two distinct ways, leading to the *Fddd* and *Pnna* network symmetries.

In summary, we have demonstrated that the triply continuous O^{70} network phase is destabilized by large amplitude reciprocating shear, with subsequent growth of O^{52}, a single crystal network phase, upon cessation of flow. To our knowledge this sort of field-induced network-to-network phase transition is unprecedented in soft condensed matter. This result underscores the delicate nature of block copolymer phase behavior, and, in particular, linear *ABC* triblocks, where candidate morphologies are spaced closely together on the free energy surface. Small, symmetry breaking perturbations are capable of trapping long-lived nonequilibrium morphologies.

We acknowledge support for this work from the NSF through Grant No. DMR-0220460. Use of the Advanced Photon Source was supported by the U.S. Department of Energy, Basic Energy Sciences, Office of Science, under Contract No. W-31-109-Eng-38. The National Institute of Standards and Technology, U.S. Department of Commerce, is recognized for providing the neutron research facilities used in this work. We have also made extensive use of the MRSEC (NSF) supported Institute of Technology Characterization Facility at the University of Minnesota.

*To whom correspondence should be addressed.
Email address: bates@cems.umn.edu.

[1] W. Richtering, G. Schmidt, and P. Lindner, Colloid Polym. Sci. **274**, 85 (1996).
[2] U. Olsson and K. Mortensen, J. Phys. II (France) **5**, 789 (1995).
[3] W. R. Burghardt, Macromol. Chem. Phys. **199**, 471 (1998).
[4] A. B. D. Brown and A. R. Rennie, Phys. Rev. E **62**, 851 (2000).
[5] K. Krishnan *et al.*, Phys. Rev. Lett. **87**, 098301 (2001).
[6] Z. Hong, M. T. Shaw, and R. A. Weiss, Polymer **41**, 5895 (2000).
[7] K. A. Koppi, M. Tirrell, and F. S. Bates, Phys. Rev. Lett. **70**, 1449 (1993).
[8] M. E. Vigild, M. Sugiyama, K. A. Chaffin, and F. S. Bates, Macromolecules **34**, 951 (2001).
[9] K. A. Koppi *et al.*, J. Rheol. (N.Y.) **38**, 999 (1994).
[10] A. V. Zvelindovsky, G. J. A. Sevink, and J. G. E. M. Fraaije, Phys. Rev. E **62**, R3063 (2000).
[11] S. Stangler and V. Abetz, Rheol. Acta **42**, 569 (2003).
[12] J. M. Sebastian, W. W. Graessley, and R. A. Register, J. Rheol. (N.Y.) **46**, 863 (2002).
[13] D. A. Hajduk *et al.*, J. Chem. Phys. **108**, 326 (1998).
[14] M. E. Vigild *et al.*, Macromolecules **31**, 5702 (1998).
[15] L. Zhu *et al.*, Phys. Rev. Lett. **86**, 6030 (2001).
[16] T. S. Bailey, C. M. Hardy, T. H. Epps III, and F. S. Bates, Macromolecules **35**, 7007 (2002).
[17] T. H. Epps III *et al.* (unpublished).
[18] A. F. Wells, *Three-Dimensional Nets and Polyhedra, Wiley Monographs in Crystallography* (John Wiley & Sons, Inc., New York, 1977).
[19] E. W. Cochran, D. C. Morse, and F. S. Bates, Macromolecules **36**, 782 (2003).
[20] T. Tepe *et al.*, Macromolecules **28**, 3008 (1995).
[21] M. Wohlgemuth, N. Yufa, J. Hoffman, and E. L. Thomas, Macromolecules **34**, 6083 (2001).